INORGANIC CHEMISTRY
FRONTIERS

RESEARCH ARTICLE

View Article Online
View Journal | View Issue

Cite this: *Inorg. Chem. Front.*, 2021, **8**, 2549

Diversifying the luminescence of phenanthro-diimine ligands in zinc complexes†

Diana Temerova, ‡[a] Kristina S. Kisel, ‡[a,b] Toni Eskelinen, [a] Alexei S. Melnikov,[c] Niko Kinnunen, [a] Pipsa Hirva, [a] Julia R. Shakirova, [b] Sergey P. Tunik, [b] Elena V. Grachova [b] and Igor O. Koshevoy *[a]

Strongly blue fluorescent 1-phenyl-2-(pyridin-2-yl)-1*H*-phenanthro[9,10-*d*]imidazole (**L1**) is a facile block for the construction of multichromophore organic molecules, and simultaneously serves as a chelating diimine ligand. The coordination of **L1** to zinc halides enhances the intraligand charge transfer and decreases the emission energy. For the iodide derivative, intra- and intermolecular heavy atom effects lead to a dual singlet–triplet emission with a temperature-dependent ratio of fluorescence and phosphorescence bands in the crystalline state. Decoration of the anthracene core with pyridyl-phenanthroimidazole units (**L2** and **L3**) changes the localization of the lowest energy electronic transitions to the former polyaromatic motif. The solid-state photophysical characteristics of **L2** and **L3**-based compounds strongly depend on the intermolecular interactions between the constituting π-systems (phenanthrene and anthracene), which are perturbed by the ZnX_2 coordinated fragments. Modulation of π-stacking contacts in these molecular materials containing **L2** and **L3** chromophores forms a basis for dynamic optical properties, responsive to mechanical, thermal, or chemical stimuli.

Received 2nd February 2021,
Accepted 12th March 2021

DOI: 10.1039/d1qi00149c

rsc.li/frontiers-inorganic

Introduction

Organic platforms, which offer a range of molecular materials with versatile solid-state photophysical behavior without tedious synthetic modifications, are particularly attractive systems for the development of tunable and stimuli-responsive luminophores.[1–8] An efficient and straightforward approach to influence the electronic structures of π-conjugated chromophores and to modulate intermolecular interactions is the employment of coordination bonding. In this respect, readily available Zn(II) salts are considered as attractive and inexpensive modifiers of organic emitters decorated with nitrogen and oxygen donor functions. Due to the stable d^{10} closed shell configuration, the zinc(II) metal center does not participate in the metal to ligand charge transfer upon electronic excitation. Therefore, the complexation of an organic motif with the Zn(II) ion typically enhances intra-ligand fluorescence as a result of increased molecular rigidity and suppression of photoinduced electron transfer reactions. The binding of this metal can also perturb the intramolecular charge transfer (ICT) that distinctly changes the emission energy of the complex compared to that of the free ligand.[9–12] Besides, the coordination-driven assembly of two or more chromophore ligands can lead to secondary interactions between the corresponding π-systems and produce aggregates with dynamic optical properties and interligand charge-transfer processes.[13–15] In solution, such easily detectable responses allow for efficient luminescence sensing of the Zn(II) ion by a variety of organic probes.[16–22]

In the solid state, in addition to intramolecular effects, the non-covalent intermolecular interactions, *e.g.* hydrogen/halogen bonding and π-stacking, govern the organization of the constituting conjugated moieties, and often play a decisive role in modulating the physical characteristics of the bulk materials.[23] It is not surprising that the combination of a metal ion or of a simple MX_n fragment with an extended π-molecule has a strong influence on the supramolecular arrangement of organic building blocks, and introduces supplementary intermolecular connectivity with the participation of the metal cation and X anions.[24] For instance, the complexation of an amine-functionalized pyridinyl-pyrazole ligand with $ZnCl_2$ shows an efficient alteration of the hydrogen bonding network and of the phase behavior caused by the metal halide unit.[25] Tuning the π–π stacking contacts between

[a]*Department of Chemistry, University of Eastern Finland, Joensuu, 80101, Finland. E-mail: igor.koshevoy@uef.fi*
[b]*St Petersburg State University, Department of Chemistry, Universitetskii pr. 26, 198504, St Petersburg, Russia*
[c]*Centre for Nano- and Biotechnologies, Peter the Great St Petersburg Polytechnic University, 195251 St Petersburg, Russia*

†Electronic supplementary information (ESI) available: Synthesis, computational and photophysical details. CCDC 2060299–2060311. For ESI and crystallographic data in CIF or other electronic format see DOI: 10.1039/d1qi00149c

‡Equal contribution.

the chromophores of a chiral pyrene-containing histidine by means of Zn(II) coordination has been used to switch the circularly polarized luminescence of the nanoassemblies.[26] On the other hand, packing-assisted heteroleptic π-interactions between electron-poor and -rich ligands can yield solid donor–acceptor complexes with improved charge transfer properties.[27] Furthermore, dense π–π stacking between aromatic linkers in Zn(II)-assembled metal–organic frameworks and coordination polymers has been identified as an important factor for enhancing long room temperature phosphorescence (RTP).[28–30] In general, triplet emission rarely occurs in zinc complexes under ambient conditions because of the inefficient spin–orbit coupling (SOC) and small heavy atom effect (HAE) caused by this metal ion;[31,32] the majority of the reported examples of phosphorescent materials correspond to the polymer-like species.[28–30,33–38] To solve this problem, a recently proposed approach to increase the SOC, promote intersystem crossing (ISC) and populate the triplet excited state, relying on an external HAE induced by Zn-bound heavier halides or halide counterions has been applied.[32,39,40] This facile strategy, which does not require modification of the organic ligand by forming covalent C–Br/I bonds, allowed RTP with quantum yields of up to 9%.[39] It is noteworthy that the effect of intermolecular interactions on the photoluminescence properties of organic molecular materials is frequently manifested by remarkable mechano-, vapo- and thermo-responsive behaviors, which can be triggered or tuned as well through the coordination to various metal ions including zinc(II).[41–44]

In the current work, we have selected a family of easy to prepare phenanthrene-based pyridyl-imidazole ligands and their anthracene derivatives (Fig. 1), which are known to be fluorescent in solution.[45] Binding these chromophores to some ZnX_2 salts (X = Cl, I, OAc) has a substantial impact on the solid state photophysical behavior. A range of intermolecular contacts were found to be subtly dependent on the anions X and allowed realizing such phenomena as temperature-variable dual emission and mechanochromic luminescence, which could not be attained for the parent organic compounds.

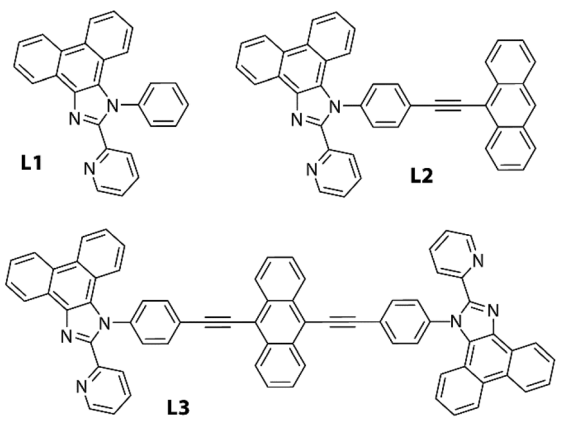

Fig. 1 Ligands **L1**–**L3** used in this study.

Results and discussion

Preparation of zinc complexes

Ligands **L1** and **L2**, containing a pyridyl-imidazole coordinating function fused with a polyaromatic phenanthrene motif, were readily obtained as described earlier.[45,46] **L3**, which comprises diethynylanthracene decorated with two diimine motifs, was synthesized in a good yield analogously to **L2** (Scheme S1, see the experimental details in the ESI†).

The coordination of congener bidentate pyridyl-imidazole ligands to zinc(II) ions has been described previously for a number of polymeric and molecular complexes.[47–54] Treatment of ligands **L1**–**L3** with ZnX_2 salts in dichloromethane/methanol or diethyl ether mixtures at room temperature afforded the corresponding complexes Zn(**L1**)X_2 (**1X**, X = Cl **1Cl**, I **1I**, OAc **1OAc**), Zn(**L2**)X_2 (**2X**, X = Cl **2Cl**, I **2I**, OAc **2OAc**) and Zn_2(**L3**)$(OAc)_4$ (**3OAc**), which were isolated as stable crystalline solids (75–97%), Scheme 1. The halide congeners of **3OAc** are very poorly soluble that prevented their purification and characterization. The ^{1}H NMR spectra of the halide complexes measured in chloroform show well-resolved patterns, which indicate that these species retain the proposed structures in solution (Fig. S1–S3†).

The acetate compounds, particularly **2OAc** and **3OAc**, show concentration dependent behavior in solution, which is tentatively attributed to the reversible dissociation of $Zn(OAc)_2$ motifs. Similar coordination–decoordination has been observed for a terpyridine-derived complex.[9] Thus, in the case of **2OAc**, lowering the concentration ultimately allows the identification of the signals of the free ligand (Fig. S2†) that confirms the hypothesis. The presence of two metal centers in **3OAc** essentially leads to somewhat different dynamics and explains the lack of ligand **L3** in a solution of the complex. It should be mentioned that multiple recrystallizations of **3OAc**

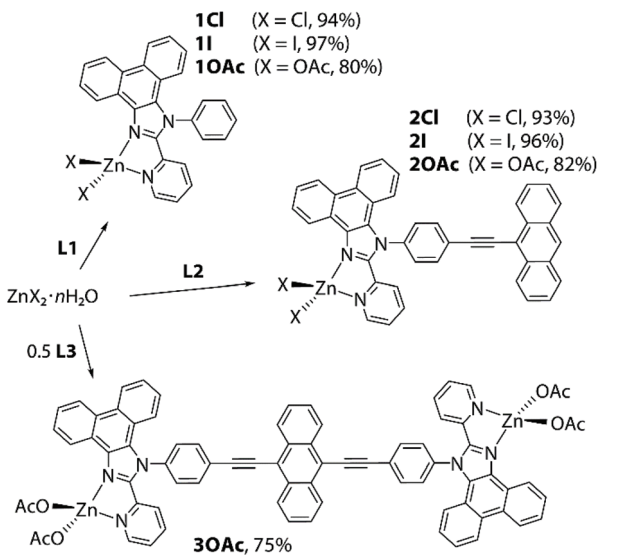

Scheme 1 Synthesis of the ZnX_2 complexes with **L1**–**L3** ligands (reaction conditions: methanol or diethyl ether/dichloromethane, 2 h, 298 K).

result in the appearance of substantial amounts of uncoordinated **L3**, which is in line with the limited stability of zinc acetate compounds **1–3OAc** in solution.

Photophysical studies in solution

The optical properties of **L1** and **L2** were described in an earlier publication.[45] The lowest energy absorption and emission bands of **L1** are assigned to a mixture of $\pi_{phen} \rightarrow \pi^*_{phen}/\pi^*_{py}$ transitions. The coordination of zinc halide units to **L1** causes a bathochromic shift of bands in both **1Cl** and **1I** (Table 1 and Fig. 2), which is in accordance with the reported effect of zinc complexation.[55–58] The metal perturbation evidently leads to an appreciable $\pi_{phen} \rightarrow \pi^*_{py}$ intraligand charge transfer (ILCT) character and stabilization of the π^*_{py} orbitals (LUMO) as confirmed by TD-DFT analysis (see the predicted low energy excitations and frontier molecular orbitals of **1X** in Table S1† and Fig. 3, S4†). These ILCT transitions, which predominantly occur between the HOMO and the LUMO, account for the disappearance of the vibronic structure of the main emission band of these complexes (λ_{em} = 430–434 nm). The calculated wavelengths of **1Cl** and **1I** correlate well with the predicted values (Table S2†). Both **1Cl** and **1I** show a weak emission band at 371 nm that presumably corresponds to the free ligand due to some degree of dissociation, although the presence of **L1** was not detected in the NMR spectra of these complexes. The lifetime measured at the major band and quantum yield of **1Cl** (Φ_{em} = 0.45, τ_{obs} = 2.3 ns) are close to those of the free ligand, and expectedly confirm the fluorescence origin of the emission. Such behavior in solution is typical of zinc(II) diimine complexes, which exhibit intraligand fluorescence, somewhat bathochromically shifted, often with higher intensity compared to that of the parent ligands.[58–61] Halide ligands at the zinc metal show little influence on the emission wavelength of **1Cl** and **1I**, but drastically affect the intensity of emission that has also been noticed for the related ZnX_2 (X = Cl, I) compounds.[55] Replacing chloride with iodide decreases the quantum yield from 0.45 (**1Cl**) to 0.02 (**1I**).

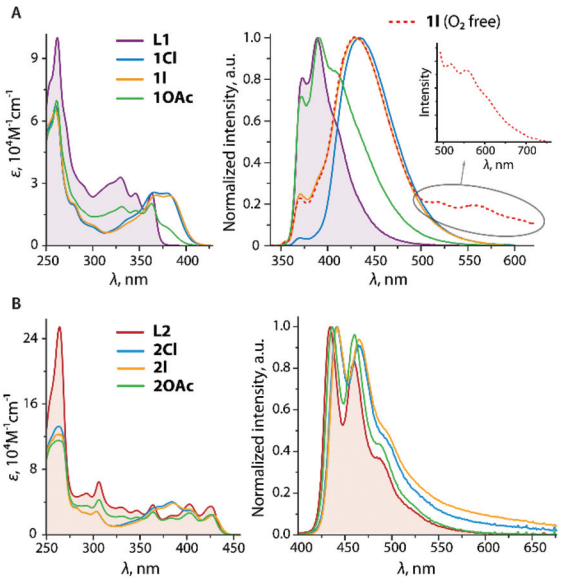

Fig. 2 Absorption (left) and normalized emission (right) spectra of **L1** (filled graphs), **1X** (A) and **L2**, **2X** (B) recorded in 1,2-dichloroethane (298 K).

Under oxygen-free conditions, a rather weak lower energy band (λ_{em} = 518, 555 nm) can be detected for **1I** (Fig. 2, the decay profile is shown in Fig. S5†). A long lifetime of 2.7 μs suggests that this signal arises from the triplet manifold with substantial ligand-centered nature (*i.e.* $^3\pi\pi^*$), as pointed by discernible vibronic progression (*ca.* 1290 cm^{-1}).

The decrease of the fluorescence intensity for **1I** and the appearance of the triplet emission indicate that a rather fast ISC ($S_1 \rightarrow T_n$) takes place resulting in the population of the triplet excited state. This process is likely facilitated by the internal heavy atom effect caused by two iodine ligands. According to the population analysis, the HOMO and the LUMO of **1I** (Fig. 3), which constitute 98% of the $S_0 \rightarrow S_1$ tran-

Table 1 Photophysical properties of ligands **L1–L3** and their zinc complexes in solution (1,2-dichloroethane, 298 K)

	λ_{abs}, nm (ε, 10^4 M^{-1} cm^{-1})	λ_{em},[a] nm	Φ	τ, ns	k_r,[b] s^{-1}	k_{nr},[c] s^{-1}
L1[d 45]	261 (10.0), 316 (3.0), 330 (3.3), 346 (2.5), 362 (2.5)	370, 388	0.37	1.9	1.9×10^8	3.3×10^8
1Cl	261 (6.8), 367 (2.6), 379 (2.6)	371, 434	0.45	2.3	2.0×10^8	2.4×10^8
1I	260 (7.6), 369 (2.8), 382 (2.8)	371, 430, (518, 555)[e]	0.02[f]	<1@433 nm (2700@560 nm)[e]		
1OAc	262 (6.8), 322 (2.2), 347 (2.1), 363 (2.4)	372, 390, 407	0.57	2.2	2.6×10^8	2.0×10^8
L2[d 45]	264 (25.4), 292 (5.2), 306 (6.4), 330 (3.4), 347 (3.0), 363 (3.7), 402 (3.8), 425 (3.6)	433, 459, 486	0.65	3.3	2.0×10^8	1.1×10^8
2Cl	262 (13.3), 303 (2.9), 384 (4.1), 429 (2.5)	442, 465	0.40	6.4	6.3×10^7	9.4×10^7
2I	263 (12.3), 303 (2.9), 385 (3.9), 429 (2.5)	442, 465	0.20	5.4	3.7×10^7	1.5×10^8
2OAc	263 (11.6), 306 (4.3), 364 (2.8), 402 (2.7), 426 (2.5)	436, 460, 487	0.58	3.6	1.6×10^8	1.2×10^8
L3	262 (14.1), 274 (13.4), 319 (8.2), 346 (3.4), 363 (3.5), 447 (4.6), 473 (5.0)	486, 515, 550sh[g]	0.60	2.6	2.3×10^8	1.5×10^8
3OAc	262 (17.3), 274 (15.7), 319 (8.0), 345 (3.5), 363 (3.8), 447 (4.8), 473 (5.2)	485, 516, 550sh[g]	0.65	2.6	2.5×10^8	1.3×10^8

[a] λ_{exc} 365 nm for **1Cl**, **L3** and **3OAc** and λ_{exc} 330 nm for other compounds. [b] k_r values were estimated by Φ/τ_{obs}. [c] k_{nr} values were estimated by $(1 - \Phi)/\tau_{obs}$. [d] Emission data in dichloromethane from ref. 45. [e] Data obtained under deaerated conditions. [f] In aerated solution. [g] sh stands for shoulder.

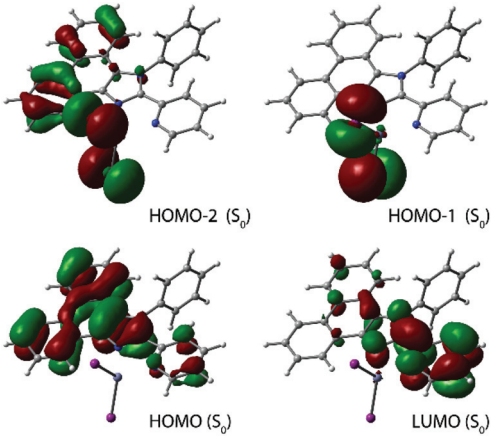

Fig. 3 Frontier molecular orbitals for the ground states of complex **1I** (in chloroform, the singly occupied orbitals for S_1 and T_1 states are shown in Fig. S4†).

sition (f = 0.54, Table S1†), are distributed over the pyridylimidazole and phenanthrene motifs (21% and 76% for the HOMO, 83% and 14% for the LUMO) with a minor contribution of the iodides (3% for the HOMO). Also, the ZnI_2 unit plays a negligible role in the formation of the lowest and the highest singly occupied molecular orbitals (LSOMO and HSOMO) predicted for the S_1 and T_1 states (Fig. S4†). The iodides, however, have a major contribution to the HOMO−1/−2 (Fig. 3) and might account for some admixture of the halide → π* charge transfer (XLCT) in the excitation and increase the SOC. It should be mentioned that only a few zinc complexes have demonstrated phosphorescence in solution under ambient conditions.[31,62]

The absorption and emission profiles of **1OAc** (Fig. 2) are generally closer to those of the free ligand **L1**, and show only some contribution of low energy charge transfer transitions that reflects a weaker binding of the $Zn(OAc)_2$ motif and its relatively easy dissociation in solution.

In the case of **L2**[45] and **L3**, the electronic transitions between the HOMO and LUMO, which are localized within the polyaromatic anthracene chromophore and the phenyleneacetylene spacers (Fig. 4), are responsible for the excitation and emission.

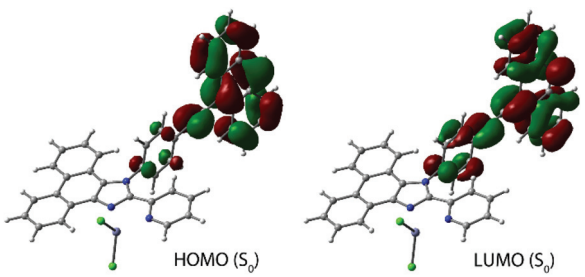

Fig. 4 Frontier molecular orbitals of complex **2Cl** (in chloroform).

Symmetrical substitution of anthracene in **L3** results in some extension of the conjugated π-system, and therefore decreases the optical band gap ΔE_{calc} (HOMO–LUMO) to 2.9 eV compared to that of **L2** (3.3 eV). Overall, the fluorescence spectra of these ligands (Fig. 2 and 5) resemble those of the corresponding phenylethynyl anthracences.[63] Due to the lack of electronic communication of the emissive motif with the metal-coordinating parts of the ligand, the emission bands of the ligands **L2** and **L3** and respective zinc complexes **2X**, **3OAc** (Fig. 2 and 5) are very similar and reveal the clearly resolved vibrational structure arising from their $\pi\pi^*_{an}$ character (Table S1;† Fig. 4, S6 and S7†). The effect of metal binding to **L2** and **L3** on the photophysics is mainly seen in a decrease in the quantum yield of halides, Φ_{em} **L2** > **2Cl** > **2I**, which probably suggests some excitation energy transfer to the predominantly dark triplet state of the phenanthroimidazole fragment.

Structural and photophysical studies in the solid state

The pertinent luminescence data are listed in Table 2. The emission properties of the titled complexes in the solid state substantially depend on the molecular packing, and therefore their discussion is carried out together with systematic crystal-

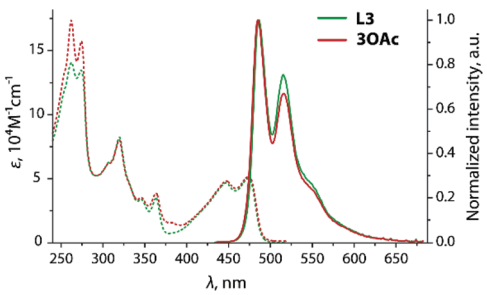

Fig. 5 Absorption (dotted lines) and normalized emission (solid lines) spectra of **L3** and **3OAc** recorded in 1,2-dichloroethane (298 K).

Table 2 Photophysical properties of ligands **L1**–**L3** and their zinc complexes in the solid state (298 K)

	λ_{em} nm	Φ	τ, ns[a]	k_r,[b] s^{-1}	k_{nr},[c] s^{-1}
L1	413	0.12	3.0	4.0×10^7	2.9×10^8
1Cl_a	460	0.28	2.7	1.0×10^8	2.7×10^8
1Cl_b	464(sh), 473	0.19	1.7	1.1×10^8	4.8×10^8
1I_a	469	0.01	0.5	2.0×10^7	2.0×10^9
1I_b	470, 554, 596	0.03	1.0, 10^5		
1OAc	478	0.14	2.0[c]	7.0×10^7	4.3×10^8
L2	497	0.03	2.9	1.0×10^7	3.3×10^8
2Cl	471	0.03	1.6	1.9×10^7	6.1×10^8
2I	506(sh), 598	0.06	1.3, 3.6		
2OAc	497	0.02	1.6	1.3×10^7	6.1×10^8
L3_y (yellow)	543	0.04	2.6	1.5×10^7	3.7×10^8
L3_r (red)	597	0.03	2.3	1.3×10^7	4.2×10^8
3OAc_y	562	0.03	3.5	8.6×10^6	2.8×10^8
3OAc_r	611	0.06	3.4	1.8×10^7	2.8×10^8

[a] Average emission lifetime for the two exponential decay $\tau_{av} = (A_1\tau_1^2 + A_2\tau_2^2)/(A_1\tau_1 + A_2\tau_2)$, A_i are pre-exponential factors. [b] k_r values were estimated by Φ/τ_{obs}. [c] k_{nr} values were estimated by $(1 - \Phi)/\tau_{obs}$.

lographic analysis. The crystal data are summarized in Tables S3 and S4,† powder diffraction patterns are presented in Fig. S8.† In all complexes, zinc atoms are found in a typical pseudo tetrahedral coordination environment, comprising two nitrogen donors forming a five membered chelate ring, and two halide or acetate ligands. The pyridyl ring and the phenanthroimidazole system are expectedly virtually in the same plane, together with the metal center. The bond lengths and angles around the zinc ion (Tables S5 and S6†) are not exceptional and lie in the range determined for similar compounds.[9,25,55,58] In view of the photophysical behavior of bulk crystalline samples, we mainly focus on the mutual arrangement of the chromophores and their intermolecular interactions.

L1 and 1X series. The fluorescence of crystalline **L1** (λ_{em} = 413 nm, Φ_{em} = 0.12, Fig. 6) is less intense and is slightly red shifted with respect to the characteristics of 1,2-dichloroethane solution ($\lambda_{em\ max}$ = 388 nm, Φ_{em} = 0.37). In the absence of stacking interactions in the structure of **L1**,[45] the radiative relaxation is evidently of an intramolecular ππ* nature as in the fluid medium.

Crystallization of compounds **1X** resulted in different modifications depending on the solvents used. The solvatomorphs of the chloride, **1Cl_a** (dichloromethane solvate) and **1Cl_b** (chloroform solvate), exhibit noticeable π-stacking interactions between the phenanthrene systems (Fig. S9†).

The acetate **1OAc** (Fig. S10†) and the dichloromethane solvate of the iodide complex **1I_a** (Fig. 7) show π–π contacts, which involve both polyaromatic and the pyridine motifs of adjacent molecules. However, the emission maxima of these crystalline species demonstrate a rather minor variation (λ_{em} = 460–478 nm, Fig. 6) indicating that stacking in this case has a moderate influence on the properties of the excited state. Analogously to the solution behavior, the luminescence of **1X** in the solid form is manifested by broad structureless bands, which are observed at lower energies than those of the parent **L1**. The excitation spectra of **L1** and **1X** (Fig. S11†) follow the same trend that complies with the change in the nature of the S_1 state of complexes and the substantial ILCT character of the emission of **1X**. The chloride and acetate compounds **1X** are somewhat more efficient fluorophores (Φ_{em} = 0.14–0.28) than the free ligand primarily due to the increased radiative decay rate of *ca.* 1.0×10^8 s^{-1} (Table 2). As in solution, the iodide **1I** in the solid state (in both forms **1I_a** and **1I_b**) exhibits the lowest quantum yield due to the ISC ($S_1 \rightarrow T_n$) transition to the dark triplet state, similar to zinc halide compounds with pyridylimidazo-pyridine ligands.[55] While **1I_a** does not show room temperature phosphorescence, the solvent-free modification to **1I_b** is dually emissive (Fig. 6). It demonstrates a dominating high energy fluorescence band (λ_{em} = 470 nm), which is accompanied by a low energy structured signal (λ_{em} = 554, 596; total Φ_{em} = 0.03) with a long observed lifetime of *ca.* 100 μs. In contrast to **1I_a**, no appreciable π-interactions are seen in **1I_b**. Instead, **1I_b** forms short intermolecular contacts I···π (*ca.* 3.5 Å, Fig. 7) between the iodide ligand and the imidazole ring

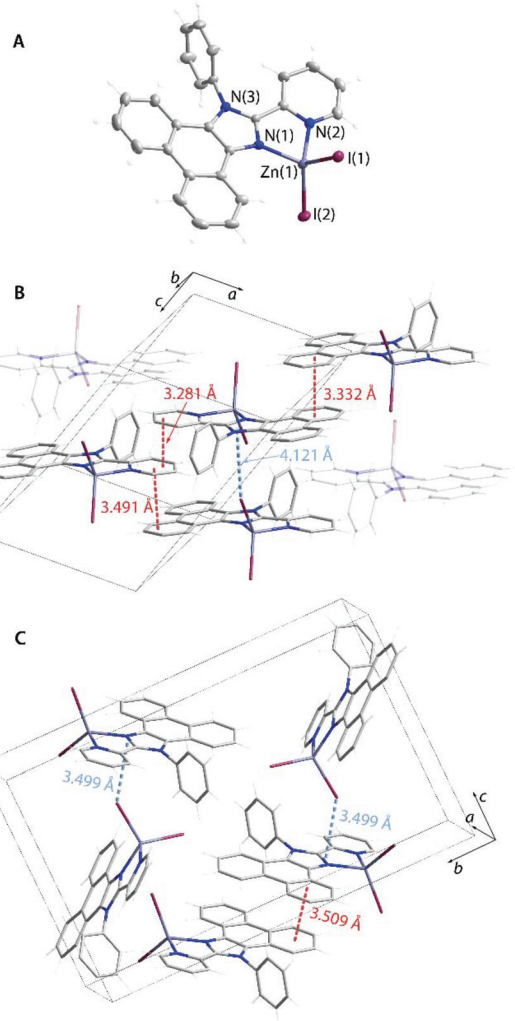

Fig. 7 Molecular view of **1I_a** (A), and packing fragments of **1I_a** (B) and of **1I_b** (C). Crystallization dichloromethane molecules in **1I_a** are omitted for clarity. The intermolecular π–π distances are measured between the planes of the phenanthrene motifs. The intermolecular π–I distance is measured between I and the imidazole plane. Thermal ellipsoids are shown at the 50% probability level.

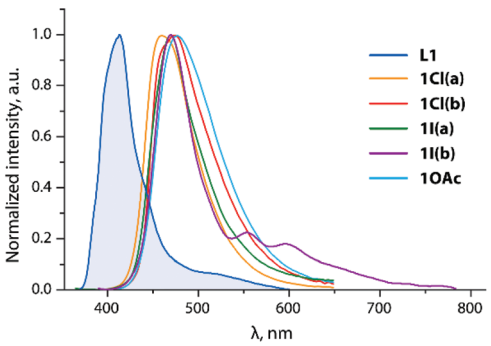

Fig. 6 Normalized solid state emission spectra of **L1** (filled graph) and **1X** (298 K, λ_{exc} = 350 nm).

(*cf.* 4.121 Å for analogous separation in **1I_a**). This unique arrangement presumably accounts for the enhancement of the external HAE in **1I_b** that causes larger SOC and results in detectable intraligand triplet emission under ambient conditions. The importance of the HAE and of close halide···chromophore contacts in promoting SOC has been recently shown for zinc halide coordination polymers prepared *via* a 1,3,5-tris (1-imidazolyl)benzene luminescent linker.[38]

Decreasing the temperature has a drastic influence on the ratio of fluorescence and phosphorescence intensities of form **1I_b** (Fig. 8A and Table S7†). Upon cooling the crystals of **1I_b**, the low energy band shows a drastic growth that produces white-orange luminescence, whereas the observed lifetime of the red shifted band increases from *ca.* 100 μs at 298 K to 2.2 ms at 77 K. Taking into account that SOC induced by the HAE is proportional in the first approximation to Z^4/r^3 (Z is the atomic number and r is the distance between the chromophore and the heavy atom),[64] and then the rate of ISC, $k_{isc} \propto |\Psi_{T_1}|\hat{H}_{SO}|\Psi_{S_1}|^2/(\Delta E_{S_1-T_1})^2$, is related to the distance as $1/r^6$. This implies that the probability of populating the T_1 state is highly sensitive to intermolecular separation for **1I_b** assuming the external HAE.

To assess the correlation of the emission with the structural parameters and temperature, we performed variable-temperature XRD studies. Indeed, the intermolecular distance I···π_{imi} is nearly linearly dependent on the temperature and decreases from 3.572 Å at 295 K to 3.499 Å at 150 K (Fig. 8B, Table S7†) that could be one of the decisive factors that determines the increase of phosphorescence *vs.* fluorescence. In addition to the triplet luminescence, which is uncommon for zinc complexes,[31,32,65,66] **1I_b** represents an interesting example of a reversibly responsive material, the emission color of which (Fig. 8C) is regulated by the temperature-dependent ratio of the singlet and triplet radiative decays.

Form **1I_a** also exhibits luminescence thermochromism (Fig. S12†), although in a less pronounced manner compared to **1I_b**. In the absence of short I···π contacts, a notable increase of the phosphorescence band of **1I_a** starts at around 150 K that can be attributed to the rigidification of the structure and moderate intra- and intermolecular heavy atom effects.

L2 and 2X series. The emission of the solid ligand **L2** (λ_{em} = 497 nm, Fig. 9A) is unstructured and is found at a longer wavelength in comparison with that in solution (λ_{em} = 433 nm,

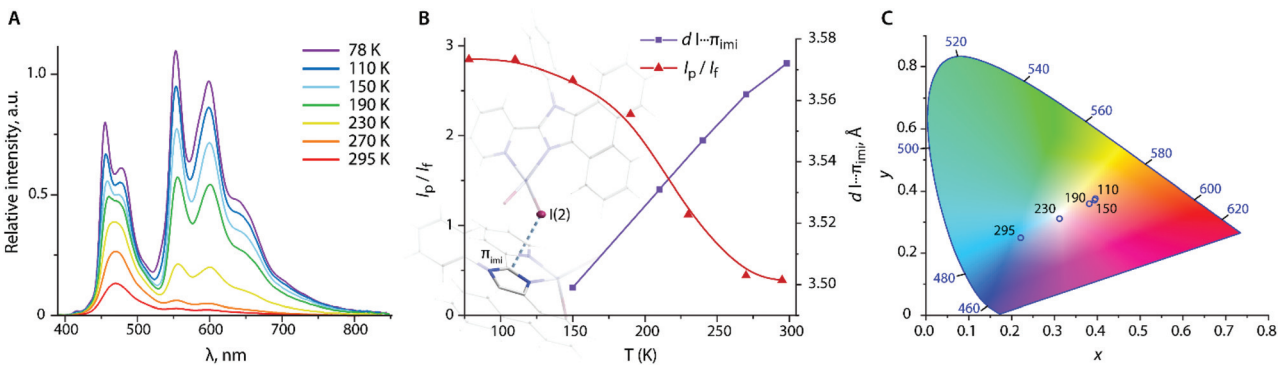

Fig. 8 (A) Variable temperature solid state emission spectra of **1I_b**; (B) temperature dependences of the ratio of intensities of the phosphorescence and fluorescence bands (I_p/I_f), and of the intermolecular distance between the iodine atom and the plane of imidazole (d I···π_{imi}); and (C) CIE 1931 coordinates of the emission of **1I_b** at different temperatures.

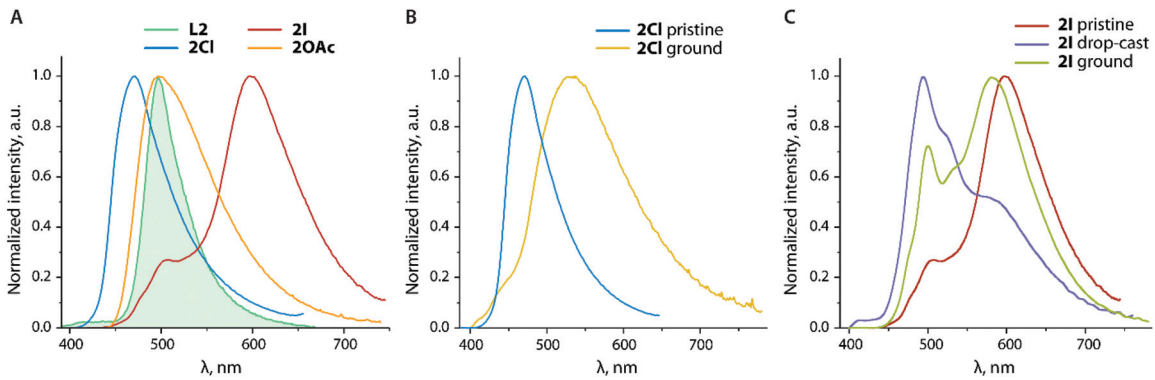

Fig. 9 Normalized solid state emission spectra of (A) **L2** (filled graph) and **2X** (298 K, λ_{exc} = 400 nm for **2I**, λ_{exc} = 350 nm for other samples); (B) pristine and ground **2Cl** (298 K); and (C) pristine, ground and dropcast **2I** (298 K).

Fig. 2). Substantial quenching of luminescence in the solid state (*ca.* 20-fold decrease *vs.* solution, Table 1) and the decrease in energy likely arise from certain π-interactions between the chromophore anthracene fragments, however, the assignment to either perturbed monomer or excimer emission is ambiguous on the basis of the available data.[67,68] The quantum yield, observed lifetimes, and the excitation and emission profiles of **L2** and **2OAc** are very similar (Fig. 9 and S13†), whereas the fluorescence maxima nearly coincide that suggests resembling resemblance in the packing and the nature of the excited states. The hypsochromic shift of the fluorescence band of the crystalline chloride complex **2Cl** (λ_{em} = 471 nm, Fig. 9A) confirms the monomer anthracene emission. Indeed, the structure of **2Cl** (Fig. S14†) confirms that the anthracene π-system is not involved in appreciable stacking interactions, which are found between the phenanthrene fragments only. Mechanical grinding of the pristine sample **2Cl** produces an amorphous material exhibiting green-yellow luminescence (λ_{em} = 532 nm, Fig. 9B and Table S8†). Together with the visibly changed excitation spectrum (Fig. S13†), it points to the alteration of molecular packing, which conceivably results in the emergence of π-interactions between the anthracene chromophores. On the other hand, grinding of **2OAc** has a little influence on the fluorescence spectrum (Fig. S15†).

Unlike **2Cl** and **2OAc**, the crystalline iodide congener **2I** is a dual emitter with the dominating band with the maximum at 598 nm (Fig. 9A) and the observed lifetime of 3.6 ns. Such a significant red shift is not typical of anthracene excimer fluorescence.[67,69,70] The crystal structure of **2I** shows short π–π contacts between the emissive anthracene and phenanthrene fragments (Fig. 10) that makes the formation of an exciplex or intermolecular charge transfer (anthracene → phenanthroimidazole) possible. The excitation spectrum of **2I** monitored at 620 nm clearly differs from those of other **2X** species and shows an intense red shifted band (Fig. S13†) that assumes ground state aggregation. The minor high energy band in the emission of **2I** (λ_{em} = 506 nm) plausibly arises from the locally excited state, *i.e.* corresponding to the monomer anthracene luminescence. This signal might originate for instance from the surface/peripheral molecules, which experience less intermolecular interactions.[71,72] The impact of mechanical stimulus on the emission pattern of **2I** is rather moderate and results in the growth of some blue shifted bands (Fig. 9C), evidently due to the high stability of the crystalline packing mode. However, the fluorescence of a film-like sample prepared by fast evaporation of a dichloromethane solution of **2I** is essentially switched mainly to the monomer origin with the maximum at 494 nm and a distinguishable vibrational structure (*ca.* 1160 cm^{-1}) due to the lack of intermolecular interactions. The excitation spectrum of the dropcast sample **2I** is similar to those of **2OAc** and ground **2Cl**, and therefore supports the disruption of charge-transfer anthracene–phenanthrene stacking in the amorphous state.

L3 and complex 3OAc. Depending on the conditions, ligand **L3** and the zinc acetate derivative **3OAc** can be isolated by at least two modifications (see the ESI), which show distinctly different luminescence characteristics (Fig. 11). The minor yellow crystalline forms of **L3_y$_{cr}$** and **3OAc_y$_{cr}$** were structurally characterized (Fig. S16† and Fig. 12).

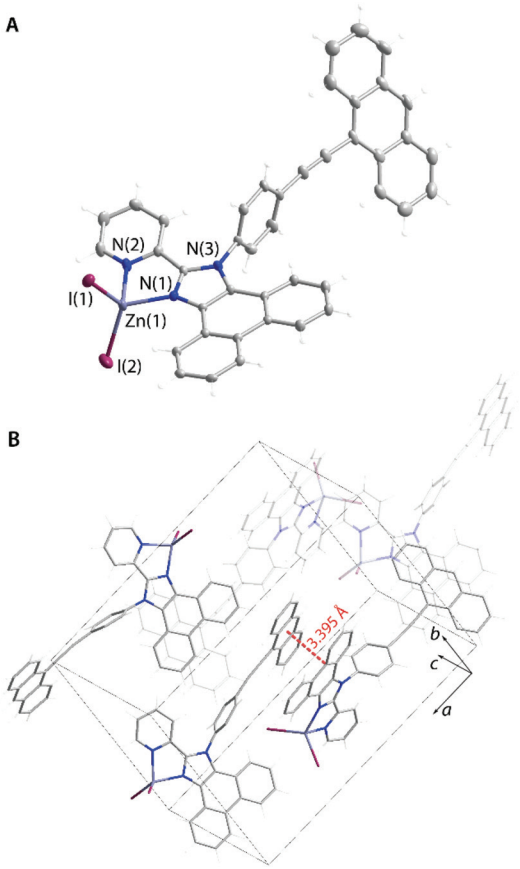

Fig. 10 Molecular view (A) and unit cell packing of **2I** (B). Crystallization of chloroform molecules are omitted for clarity. The intermolecular π–π distance is measured between the plane of the anthracene and the C(8) atom of phenanthrene. Thermal ellipsoids are shown at the 50% probability level.

Although these single crystals do not represent the bulk yellow modifications **L3_y**/**3OAc_y**, the photophysics of which was analyzed, similar colours of the samples suggest that they have similar arrangements in the solid. According to the XRD data, the diethynyl anthracene fragments of the chromophore do not show appreciable stacking interactions, and therefore the observed yellow fluorescence (λ_{em} = 543/562 nm, Φ_{em} = 0.04/0.03 for **L3_y**/**3OAc_y**) presumably corresponds to the monomer emission, broadened and red shifted with respect to the solution spectra (Fig. 5).

Although we could not obtain crystals of **L3_r**/**3OAc_r** suitable for structural analysis, the colours of these solids and of their luminescence (λ_{em} = 597/611 nm, Φ_{em} = 0.03/0.06 for **L3_r**/**3OAc_r**) propound aggregation with the involvement of the emissive anthracene centers, reminiscent of the crystalline 9,10-bis(phenylethynyl)anthracene (BPEA).[73] The emissions of both forms of the complex are visibly red shifted compared to

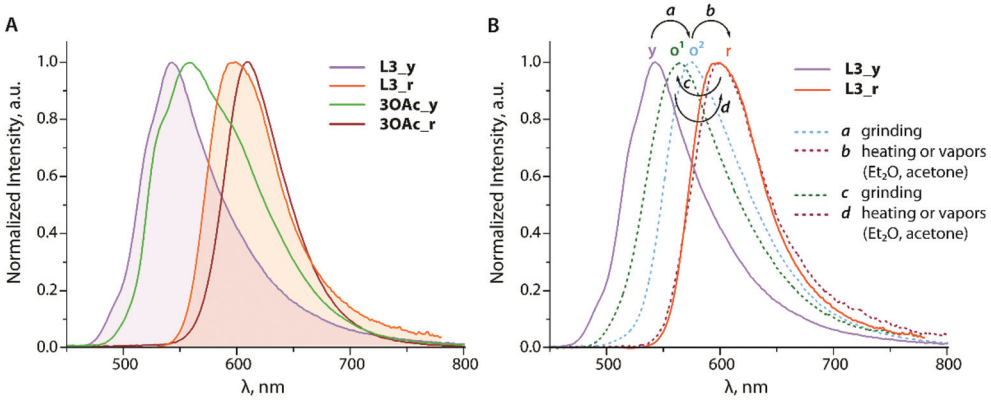

Fig. 11 Normalized solid state emission spectra of **L3** (filled graphs) and complex **3OAc** at 298 K (A) and variation of the emission spectra of **L3** under different stimuli (B).

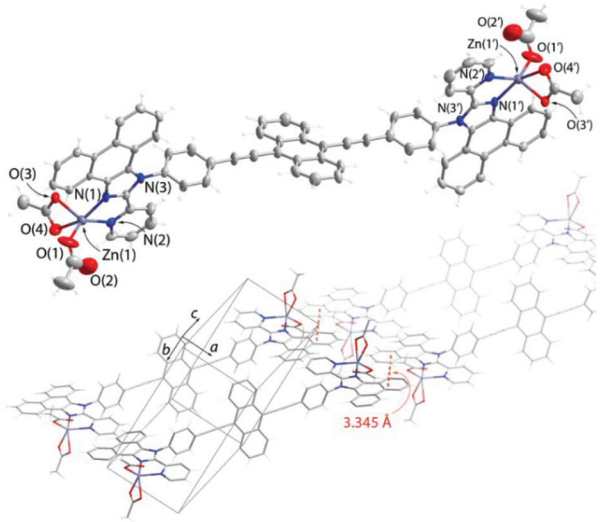

Fig. 12 Molecular view and packing fragment of **3OAc_y**. Crystallization solvent was disordered and omitted from the refinement model. The intermolecular π–π distances were measured between the planes of the phenanthrene motifs. Symmetry transformations used to generate equivalent atoms ('): $-x$, $1-y$, $-z$. Thermal ellipsoids are shown at the 50% probability level.

those of the corresponding **L3_y/r** forms of the ligand (Fig. 11A). The lowest energy maxima of the excitation spectra for the yellow and orange-red modifications vary by more than 60 nm (Fig. S17†), and thus corroborate that different molecular packings generate the excited states operating in these materials.

Ligand **L3** demonstrates distinct stimuli-responsive behaviour. Mechanical grinding of yellow **L3_y** produces a metastable orange material ($\mathbf{o}^1$, λ_{em} = 575 nm). Brief heating (up to *ca.* 300 °C) or exposure to vapors of diethyl ether further transforms this solid into the red form, the emission of which (λ_{em} = 598 nm) is nearly identical to that of the independently prepared **L3_r** (Fig. 11B). Grinding the red form leads to another metastable orange modification ($\mathbf{o}^2$, λ_{em} = 564 nm), the process is also reversible thermally by means of vapors. The transitions between different forms apparently result from the perturbation of intermolecular interactions, which involved the anthracene chromophore.

Albeit phenanthroimidazole fragments in **L3** and **3OAc** are not expected to contribute to the frontier orbitals according to the theoretical studies (Fig. S7†), apparently, they influence the intermolecular organization and mechano-/vapo-responsive behaviour. The coordinating ability of the pendant groups can be used to tune these features as the binding of zinc acetate *e.g.* bathochromically shifts the emission of both phases from 543/597 nm (**L3**) to 562/611 nm (**3OAc**, Table 2). The photophysical properties of the yellow and orange-red forms of **L3**/**3OAc** remind those of a film (yellow) and crystals (orange-red) of BPEA.[72,74] On the other hand, the fluorescence mechanochromism of some functionalized BPEA-s is clearly less expressed.[75,76]

Conclusions

In this study, we have analysed the photophysical behaviour of readily available fluorophores **L1–L3**, which comprise a pyridyl-imidazole coordinating function fused with a polyaromatic phenanthrene motif, and their zinc(II) complexes **1X–3X** derived from simple ZnX_2 salts (X = Cl, I, OAc). In solution, the optical properties of organic emitters and the corresponding metal-containing species are governed by the intraligand charge transfer and ππ* electronic transitions of the singlet parentage, localized either on the phenanthrene-diimine system (**L1** and **1X**) or within the alkynyl-anthracene chromophore fragment (**L2** and **L3**-based compounds). However, the ZnX_2 units cause little perturbance to the intraligand fluorescence of **L2** and **L3** in fluid medium, and coordination of zinc halide units to **L1** red shifts the lowest energy absorption and emission bands in **1Cl** and **1I** due to the enhanced $\pi_{phen} \rightarrow \pi^*_{py}$ CT. In the case of **1I**, the intramolecular heavy atom effect associated with iodide ligands facilitates ISC resulting in a significant decrease in the fluoresce intensity

and in the phosphorescence emission, seldom observed for zinc coordination complexes in solution.

The investigation of luminescence properties in the solid state was supported by extensive structural characterization of the title compounds. Systematic crystallographic studies highlight a strong impact of ZnX_2 groups on non-covalent intermolecular interactions, and as a consequence, on the optical features of these materials. In particular, the iodide complex **1I** demonstrates packing-dependent dual (singlet–triplet) emission, which has been correlated with short intermolecular I···π contacts. In turn, due to the temperature variability of this distance and the alteration of the phosphorescence *vs.* fluorescence ratio, the solvent-free crystals of **1I** exhibit a distinct emission color change from blue to yellow-orange in a temperature range of 150–300 K.

Switching the emissive center to the anthracene moiety in **L2** and **L3**-based species provides more possibilities for responsive properties based on the ground state π–π interactions (anthracene–phenanthrene and anthracene–anthracene). It is noteworthy that **L3** and **3OAc** exist in several forms exhibiting different fluorescence performances (λ_{em} alters from 543 to 597 nm for **L3**), which can be interconverted by means of various stimuli (mechanical and thermal treatment and exposure to a solvent). Overall, accessible preparation of organic chromophores with coordinating ability and their combination with optically innocent metal ions such as zinc offer a wide range of possibilities for the development of easy to synthesize molecular materials with diverse photophysical functionalities.

Author contributions

D. T. and K. S. K. contributed equally and performed the synthesis, and structural and NMR spectroscopic characterization. T. E. and P. H. were responsible for computational analysis. N.K. carried out PXRD measurements. K. S. K., J. R. S. and A. S. M. performed the photophysical studies. S. P. T., E. V. G. and I. O. K. planned the research.

Conflicts of interest

There are no conflicts to declare.

Acknowledgements

Financial support from the Academy of Finland (decision 317903, I.O.K.; Flagship Programme, Photonics Research and Innovation PREIN, decision 320166) and the Russian Science Foundation (grant 19-73-20055, J.R.S., photophysical studies) is gratefully acknowledged. The work was carried out using equipment of St Petersburg State University Research Park (Centres of Optical and Laser Materials Research, Chemical Analysis and Materials Research, X-ray Diffraction) and the Analytical Centre for Nano- and Biotechnologies (Peter the Great St. Petersburg Polytechnic University, with financial support from the Ministry of Education and Science of Russian Federation).

Notes and references

1 M. Shimizu and T. Hiyama, Organic Fluorophores Exhibiting Highly Efficient Photoluminescence in the Solid State, *Chem. – Asian J.*, 2010, **5**, 1516–1531.
2 Z. Chi, X. Zhang, B. Xu, X. Zhou, C. Ma, Y. Zhang, S. Liu and J. Xu, Recent advances in organic mechanofluorochromic materials, *Chem. Soc. Rev.*, 2012, **41**, 3878–3896.
3 Z. Ma, Z. Wang, M. Teng, Z. Xu and X. Jia, Mechanically Induced Multicolor Change of Luminescent Materials, *ChemPhysChem*, 2015, **16**, 1811–1828.
4 J. Mei, N. L. C. Leung, R. T. K. Kwok, J. W. Y. Lam and B. Z. Tang, Aggregation-Induced Emission: Together We Shine, United We Soar!, *Chem. Rev.*, 2015, **115**, 11718–11940.
5 X. Huang, L. Qian, Y. Zhou, M. Liu, Y. Cheng and H. Wu, Effective structural modification of traditional fluorophores to obtain organic mechanofluorochromic molecules, *J. Mater. Chem. C*, 2018, **6**, 5075–5096.
6 S. Xu, Y. Duan and B. Liu, Precise Molecular Design for High-Performance Luminogens with Aggregation-Induced Emission, *Adv. Mater.*, 2020, **32**, 1903530.
7 Y. Xie and Z. Li, The development of mechanoluminescence from organic compounds: breakthrough and deep insight, *Mater. Chem. Front.*, 2020, **4**, 317–331.
8 M. K. Bera, P. Pal and S. Malik, Solid-state emissive organic chromophores: design, strategy and building blocks, *J. Mater. Chem. C*, 2020, **8**, 788–802.
9 T. Tsukamoto, R. Aoki, R. Sakamoto, R. Toyoda, M. Shimada, Y. Hattori, M. Asaoka, Y. Kitagawa, E. Nishibori, M. Nakano and H. Nishihara, A simple zinc(II) complex that features multi-functional luminochromism induced by reversible ligand dissociation, *Chem. Commun.*, 2017, **53**, 3657–3660.
10 R. Geng, X. Hou, Y. Sun, C. Yan, Y. Wu, H.-L. Zhang and X. Shao, Driving π-plane to π-bowl through lateral coordination at room temperature, *Mater. Chem. Front.*, 2018, **2**, 1456–1461.
11 Y. Watanabe, W. Sungnoi, A. O. Sartorio, M. Zeller and A. Wei, A zinc-responsive fluorophore based on 5′-(p-hydroxyphenyl)-pyridylthiazole, *Mater. Chem. Front.*, 2020, **4**, 899–904.
12 A. Zavaleta, A. O. Lykhin, J. H. S. K. Monteiro, S. Uchida, T. W. Bell, A. de Bettencourt-Dias, S. A. Varganov and J. Gallucci, Full Visible Spectrum and White Light Emission with a Single, Input-Tunable Organic Fluorophore, *J. Am. Chem. Soc.*, 2020, **142**, 20306–20312.
13 T. Ogawa, J. Yuasa and T. Kawai, Highly Selective Ratiometric Emission Color Change by Zinc-Assisted Self-

Assembly Processes, *Angew. Chem., Int. Ed.*, 2010, **49**, 5110–5114.
14 Y. Imai and J. Yuasa, Off–off–on chiroptical property switching of a pyrene luminophore by stepwise helicate formation, *Chem. Commun.*, 2019, **55**, 4095–4098.
15 S. Iseki, K. Nonomura, S. Kishida, D. Ogata and J. Yuasa, Zinc-Ion-Stabilized Charge-Transfer Interactions Drive Self-Complementary or Complementary Molecular Recognition, *J. Am. Chem. Soc.*, 2020, **142**, 15842–15851.
16 Z. Xu, J. Yoon and D. R. Spring, Fluorescent chemosensors for Zn^{2+}, *Chem. Soc. Rev.*, 2010, **39**, 1996–2006.
17 J. Wang, W. Lin and W. Li, Single Fluorescent Probe Displays a Distinct Response to Zn^{2+} and Cd^{2+}, *Chem. – Eur. J.*, 2012, **18**, 13629–13632.
18 Y. Dong, R. Fan, W. Chen, P. Wang and Y. Yang, A simple quinolone Schiff-base containing CHEF based fluorescence 'turn-on' chemosensor for distinguishing Zn^{2+} and Hg^{2+} with high sensitivity, selectivity and reversibility, *Dalton Trans.*, 2017, **46**, 6769–6775.
19 S. Ullmann, R. Schnorr, M. Handke, C. Laube, B. Abel, J. Matysik, M. Findeisen, R. Rüger, T. Heine and B. Kersting, Zn^{2+}-Ion Sensing by Fluorescent Schiff Base Calix[4]arene Macrocycles, *Chem. – Eur. J.*, 2017, **23**, 3824–3827.
20 W. L. Turnbull and L. G. Luyt, Amino-Substituted 2,2′-Bipyridine Ligands as Fluorescent Indicators for ZnII and Applications for Fluorescence Imaging of Prostate Cells, *Chem. – Eur. J.*, 2018, **24**, 14539–14546.
21 S. N. Ansari, A. K. Saini, P. Kumari and S. M. Mobin, An imidazole derivative-based chemodosimeter for Zn^{2+} and Cu^{2+} ions through "ON–OFF–ON" switching with intracellular Zn^{2+} detection, *Inorg. Chem. Front.*, 2019, **6**, 736–745.
22 G. Ambrosi, M. Paz Clares, I. Pont, M. Formica, V. Fusi, A. Ricci, P. Paoli, P. Rossi, E. García-España and M. Inclán, Zn^{2+} and Cu^{2+} complexes of a fluorescent scorpiand-type oxadiazole azamacrocyclic ligand: crystal structures, solution studies and optical properties, *Dalton Trans.*, 2020, **49**, 1897–1906.
23 S. Varughese, Non-covalent routes to tune the optical properties of molecular materials, *J. Mater. Chem. C*, 2014, **2**, 3499–3516.
24 E. R. T. Tiekink, Supramolecular assembly based on "emerging" intermolecular interactions of particular interest to coordination chemists, *Coord. Chem. Rev.*, 2017, **345**, 209–228.
25 L. K. Hiscock, D. Joekar, B. Balonova, M. Tomas Piqueras, Z. W. Schroeder, V. Jarvis, K. E. Maly, B. A. Blight and L. N. Dawe, Structures, Phase Behavior, and Fluorescent Properties of 3-Phenyl-1-(pyridin-2-yl)-1H-pyrazol-5-amine and Its $ZnCl_2$ Complex, *Inorg. Chem.*, 2019, **58**, 16317–16321.
26 D. Niu, Y. Jiang, L. Ji, G. Ouyang and M. Liu, Self-Assembly through Coordination and π-Stacking: Controlled Switching of Circularly Polarized Luminescence, *Angew. Chem., Int. Ed.*, 2019, **58**, 5946–5950.
27 K. Prasad, D. Samanta, R. Haldar and T. K. Maji, Excitation Energy Transfer Supported Amplified Charge-Transfer Emission in an Anthracenedicarboxylate- and Bipyridophenazine-Based Coordination Complex, *Inorg. Chem.*, 2018, **57**, 2953–2956.
28 D. Li, X. Yang and D. Yan, Cluster-Based Metal–Organic Frameworks: Modulated Singlet–Triplet Excited States and Temperature-Responsive Phosphorescent Switch, *ACS Appl. Mater. Interfaces*, 2018, **10**, 34377–34384.
29 X.-G. Yang, Z.-M. Zhai, X.-M. Lu, J.-H. Qin, F.-F. Li and L.-F. Ma, Hexanuclear Zn(II)-Induced Dense π-Stacking in a Metal–Organic Framework Featuring Long-Lasting Room Temperature Phosphorescence, *Inorg. Chem.*, 2020, **59**, 10395–10399.
30 X.-G. Yang, X.-M. Lu, Z.-M. Zhai, J.-H. Qin, X.-H. Chang, M.-L. Han, F.-F. Li and L.-F. Ma, π-Type halogen bonding enhanced the long-lasting room temperature phosphorescence of Zn(ii) coordination polymers for photoelectron response applications, *Inorg. Chem. Front.*, 2020, **7**, 2224–2230.
31 K. D. Oyler, F. J. Coughlin and S. Bernhard, Controlling the Helicity of 2,2′-Bipyridyl Ruthenium(II) and Zinc(II) Hemicage Complexes, *J. Am. Chem. Soc.*, 2007, **129**, 210–217.
32 F. Kobayashi, R. Ohtani, S. Teraoka, M. Yoshida, M. Kato, Y. Zhang, L. F. Lindoy, S. Hayami and M. Nakamura, Phosphorescence at Low Temperature by External Heavy-Atom Effect in Zinc(II) Clusters, *Chem. – Eur. J.*, 2019, **25**, 5875–5879.
33 X. Yang and D. Yan, Long-afterglow metal–organic frameworks: reversible guest-induced phosphorescence tunability, *Chem. Sci.*, 2016, **7**, 4519–4526.
34 X. Yang and D. Yan, Direct white-light-emitting and near-infrared phosphorescence of zeolitic imidazolate framework-8, *Chem. Commun.*, 2017, **53**, 1801–1804.
35 X.-G. Yang, Z.-M. Zhai, X.-M. Lu, Y. Zhao, X.-H. Chang and L.-F. Ma, Room temperature phosphorescence of Mn(ii) and Zn(ii) coordination polymers for photoelectron response applications, *Dalton Trans.*, 2019, **48**, 10785–10789.
36 Y. Zhao, X.-G. Yang, X.-M. Lu, C.-D. Yang, N.-N. Fan, Z.-T. Yang, L.-Y. Wang and L.-F. Ma, {Zn6} Cluster Based Metal–Organic Framework with Enhanced Room-Temperature Phosphorescence and Optoelectronic Performances, *Inorg. Chem.*, 2019, **58**, 6215–6221.
37 X.-G. Yang, Z.-M. Zhai, X.-Y. Liu, J.-Y. Li, F.-F. Li and L.-F. Ma, Sulfur heteroatom-based MOFs with long-lasting room-temperature phosphorescence and high photoelectric response, *Dalton Trans.*, 2020, **49**, 598–602.
38 Z.-X. Liu, J.-Q. Wang, Y. Mu, Q. Wei, J.-H. Li and G.-M. Wang, Room-Temperature Phosphorescence with Variable Lifetime of Halogen-Comprising Coordination Polymers, *Inorg. Chem.*, 2020, **59**, 17870–17874.
39 J.-Q. Wang, Y. Mu, S.-D. Han, J. Pan, J.-H. Li and G.-M. Wang, Room-Temperature Phosphorescence with Excitation-Energy Dependence and External Heavy-Atom

Effect in Hybrid Zincophosphites, *Inorg. Chem.*, 2019, **58**, 9476–9481.

40 Y. Mu, J.-Q. Wang, S.-D. Han, J. Pan, J.-H. Li and G.-M. Wang, Enhanced Room-Temperature Phosphorescence of an Organic Ligand in 3D Hybrid Materials Assisted by Adjacent Halogen Atom, *Inorg. Chem.*, 2020, **59**, 972–975.

41 R. Gao, Y. Zhao, X. Yang and D. Yan, Stimuli-responsive fluorescence based on the solid-state bis[2-(2-benzothiazoly)phenolato]zinc(II) complex and its fiber thin film, *RSC Adv.*, 2015, **5**, 56470–56477.

42 T. Tsukamoto, R. Aoki, R. Sakamoto, R. Toyoda, M. Shimada, Y. Hattori, Y. Kitagawa, E. Nishibori, M. Nakano and H. Nishihara, Mechano-, thermo-, solvato-, and vapochromism in bis(acetato-κ^1O)[4′-(4-(diphenylamino)phenyl)](2,2′:6′,2″-terpyridine-κ^3N,N′,N″)zinc(II) and its polymer, *Chem. Commun.*, 2017, **53**, 9805–9808.

43 Y. Ma, Y. Dong, S. Liu, P. She, J. Lu, S. Liu, W. Huang and Q. Zhao, Chameleon-Like Thermochromic Luminescent Materials with Controllable Response Behaviors for Multilevel Security Printing, *Adv. Opt. Mater.*, 2020, **8**, 1901687.

44 L. Tom and M. R. P. Kurup, A reversible thermo-responsive 2D Zn(ii) coordination polymer as a potential self-referenced luminescent thermometer, *J. Mater. Chem. C*, 2020, **8**, 2525–2532.

45 K. S. Kisel, T. Eskelinen, W. Zafar, A. I. Solomatina, P. Hirva, E. V. Grachova, S. P. Tunik and I. O. Koshevoy, Chromophore-functionalized phenanthro-diimine ligands and their Re(I) complexes, *Inorg. Chem.*, 2018, **57**, 6349–6361.

46 K. Qiu, M. Ouyang, Y. Liu, H. Huang, C. Liu, Y. Chen, L. Ji and H. Chao, Two-photon photodynamic ablation of tumor cells by mitochondria-targeted iridium(III) complexes in aggregate states, *J. Mater. Chem. B*, 2017, **5**, 5488–5498.

47 Z.-W. Wang, C.-C. Ji, J. Li, Z.-J. Guo, Y.-Z. Li and H.-G. Zheng, Synthesis, X-ray Structures, and Fluorescent Properties of Coordination Networks Constructed from 2-(2-Pyridinyl-benzimidazolyl) Acetic Anion, *Cryst. Growth Des.*, 2009, **9**, 475–482.

48 M. G. B. Drew, D. A. Tocher, K. Chowdhury, S. Chowdhury and D. Datta, Zinc(II) mediated synthesis of an N-substituted 2-(2-pyridyl)imidazole from a 1,2-diketone and 2-(aminomethyl)pyridine and its ligational behaviour, *New J. Chem.*, 2004, **28**, 323–325.

49 H.-Y. Liu, H. Wu, J.-F. Ma, Y.-Y. Liu, B. Liu and J. Yang, SynthesesStructures, and Photoluminescence of Zinc(II) Coordination Polymers Based on Carboxylates and Flexible Bis-[(pyridyl)-benzimidazole] Ligands, *Cryst. Growth Des.*, 2010, **10**, 4795–4805.

50 C.-J. Wang, K.-F. Yue, W.-H. Zhang, J.-C. Jin, X.-Y. Huang and Y.-Y. Wang, Three new d10 coordination polymers based on 2-(2-pyridyl)benzimidazole ligand: Synthesis, structures and properties, *Inorg. Chem. Commun.*, 2010, **13**, 1332–1336.

51 A. S. Burlov, A. S. Antsyshkina, G. G. Sadkov, V. V. Chesnokov, Y. V. Koshchienko, D. A. Garnovskii, I. S. Vasil'chenko, A. I. Uraev, G. S. Borodkin, V. S. Sergienko and A. D. Garnovskii, Coordination compounds of ambidentate 1-(H)alkyl-2-(2-pyridyl)benzimidazoles. Synthesis and crystal structure, *Russ. J. Coord. Chem.*, 2010, **36**, 906–912.

52 N. Kundu, S. M. T. Abtab, S. Kundu, A. Endo, S. J. Teat and M. Chaudhury, Triple-Stranded Helicates of Zinc(II) and Cadmium(II) Involving a New Redox-Active Multiring Nitrogenous Heterocyclic Ligand: Synthesis, Structure, and Electrochemical and Photophysical Properties, *Inorg. Chem.*, 2012, **51**, 2652–2661.

53 S. Chen, R.-Q. Fan, X.-M. Wang and Y.-L. Yang, Novel bright blue emissions IIB group complexes constructed with various polyhedron-induced 2-[2′-(6-methoxy-pyridyl)]-benzimidazole derivatives, *CrystEngComm*, 2014, **16**, 6114–6125.

54 F. Li, M.-L. Sun, X. Zhang and Y.-G. Yao, Diverse Structures and Luminescence Properties of Nine Novel Zn/Cd(II)-Organic Architectures Assembled by Two Different Rigid Ligands, *Cryst. Growth Des.*, 2019, **19**, 4404–4416.

55 G. A. Ardizzoia, S. Brenna, S. Durini, B. Therrien and M. Veronelli, Synthesis, Structure, and Photophysical Properties of Blue-Emitting Zinc(II) Complexes with 3-Aryl-Substituted 1-Pyridylimidazo[1,5-a]pyridine Ligands, *Eur. J. Inorg. Chem.*, 2014, **2014**, 4310–4319.

56 X.-M. Wang, S. Chen, R.-Q. Fan, F.-Q. Zhang and Y.-L. Yang, Facile luminescent tuning of ZnII/HgII complexes based on flexible, semi-rigid and rigid polydentate Schiff bases from blue to green to red: structural, photophysics, electrochemistry and theoretical calculations studies, *Dalton Trans.*, 2015, **44**, 8107–8125.

57 X.-m. Liu, X.-y. Mu, H. Xia, L. Ye, W. Gao, H.-y. Wang and Y. Mu, Synthesis, Structures, and Luminescent Properties of d^{10} Group 12 Metal Complexes with Substituted 2,2′-Bipyridine Ligands, *Eur. J. Inorg. Chem.*, 2006, **2006**, 4317–4323.

58 G. Volpi, E. Priola, C. Garino, A. Daolio, R. Rabezzana, P. Benzi, A. Giordana, E. Diana and R. Gobetto, Blue fluorescent zinc(II) complexes based on tunable imidazo[1,5-a]pyridines, *Inorg. Chim. Acta*, 2020, **509**, 119662.

59 V. N. Kozhevnikov, O. V. Shabunina, D. S. Kopchuk, M. M. Ustinova, B. König and D. N. Kozhevnikov, Facile synthesis of 6-aryl-3-pyridyl-1,2,4-triazines as a key step toward highly fluorescent 5-substituted bipyridines and their Zn(II) and Ru(II) complexes, *Tetrahedron*, 2008, **64**, 8963–8973.

60 G. Li, D. Zhang, G. Liu and S. Pu, A highly selective fluorescent probe for Cd^{2+} and Zn^{2+} based on a new diarylethene with quinoline–benzimidazole conjugated system, *Tetrahedron Lett.*, 2016, **57**, 5205–5210.

61 J. Yuasa, A. Mitsui and T. Kawai, π–π* Emission from a tetrazine derivative complexed with zinc ion in aqueous solution: a unique water-soluble fluorophore, *Chem. Commun.*, 2011, **47**, 5807–5809.

62 A. Barbieri, G. Accorsi and N. Armaroli, Luminescent complexes beyond the platinum group: the d^{10} avenue, *Chem. Commun.*, 2008, 2185–2193.
63 F. Zhong and J. Zhao, Phenyleneanthracene derivatives as triplet energy acceptor/emitter in red light excitable triplet-triplet-annihilation upconversion, *Dyes Pigm.*, 2017, **136**, 909–918.
64 S. P. McGlynn, T. Azumi and M. Kinoshita, *Molecular Spectroscopy of the Triplet State*, Prentice-Hall, Englewood Cliffs, NJ, 1969.
65 Q.-D. Liu, R. Wang and S. Wang, Blue phosphorescent Zn (ii) and orange phosphorescent Pt(ii) complexes of 4,4′-diphenyl-6,6′-dimethyl-2,2′-bipyrimidine, *Dalton Trans.*, 2004, 2073–2079.
66 T. E. Kokina, M. I. Rakhmanova, N. A. Shekhovtsov, L. A. Glinskaya, V. Y. Komarov, A. M. Agafontsev, A. Y. Baranov, P. E. Plyusnin, L. A. Sheludyakova, A. V. Tkachev and M. B. Bushuev, Luminescent Zn(ii) and Cd(ii) complexes with chiral 2,2′-bipyridine ligands bearing natural monoterpene groups: synthesis, speciation in solution and photophysics, *Dalton Trans.*, 2020, **49**, 7552–7563.
67 H. Ihmels, D. Leusser, M. Pfeiffer and D. Stalke, Solid-State Photolysis of Anthracene-Linked Ammonium Salts: The Search for Topochemical Anthracene Photodimerizations, *Tetrahedron*, 2000, **56**, 6867–6875.
68 Y. Mizobe, M. Miyata, I. Hisaki, Y. Hasegawa and N. Tohnai, Anomalous Anthracene Arrangement and Rare Excimer Emission in the Solid State: Transcription and Translation of Molecular Information, *Org. Lett.*, 2006, **8**, 4295–4298.
69 G. E. Berkovic and Z. Ludmer, Anomalous excimer fluorescence from anthracene derivatives crystallizing in chiral crystal structures, *J. Chem. Soc., Chem. Commun.*, 1981, 768–769.
70 J. C. Amicangelo and W. R. Leenstra, Excimer Formation in the Interlayer Region of Arene-Derivatized Zirconium Phosphonates, *J. Am. Chem. Soc.*, 2003, **125**, 14698–14699.
71 T. Seko, K. Ogura, Y. Kawakami, H. Sugino, H. Toyotama and J. Tanaka, Excimer emission of anthracene, perylene, coronene and pyrene microcrystals dispersed in water, *Chem. Phys. Lett.*, 1998, **291**, 438–444.
72 Y. Yagita and K. Matsui, Size-dependent optical properties of 9,10-bis(phenylethynyl)anthracene crystals, *J. Lumin.*, 2015, **161**, 437–441.
73 A. Li, J. Wang, S. Xu, Z. Huo, Y. Geng, W. Xu and H. Cui, Distinct stimuli-responsive behavior for two polymorphs of 9,10-bis(phenylethynyl)anthracene under pressure based on intermolecular interactions, *Dyes Pigm.*, 2019, **170**, 107603.
74 B. Manna, A. Nandi and R. Ghosh, Ultrafast Singlet Exciton Fission Dynamics in 9,10-Bis(phenylethynyl)anthracene Nanoaggregates and Thin Films, *J. Phys. Chem. C*, 2018, **122**, 21047–21055.
75 Y. Matsunaga and J.-S. Yang, Multicolor Fluorescence Writing Based on Host–Guest Interactions and Force-Induced Fluorescence-Color Memory, *Angew. Chem., Int. Ed.*, 2015, **54**, 7985–7989.
76 Y. Sagara, Y. C. Simon, N. Tamaoki and C. Weder, A mechano- and thermoresponsive luminescent cyclophane, *Chem. Commun.*, 2016, **52**, 5694–5697.

